EMagPy: open-source standalone software for processing, forward modeling and inversion of electromagnetic induction data

Authors:
Paul McLachlan[1],*
Guillaume Blanchy[1]
Andrew Binley[1]

Affiliations
[1]Lancaster Environment Centre, Lancaster University, Lancaster, UK

Corresponding author
Paul McLachlan, p.mclachlan@outlook.com

Authorship statement
GB and PM wrote the code, the jupyter notebook for the cases and the manuscript. AB contributed to writing the manuscript and supervised work on the field case studies.

Code availability
The code is available under the GPL-licence at https://gitlab.com/hkex/emagpy.

Highlights (max 85 characters)

- The cumulative sensitivity forward model is limited in some cases.
- EMagPy is an open-source Python API and GUI for 1D EMI modeling/inversion.
- Application of EMagPy is illustrated through cases studies with real and synthetic data.
- Both Maxwell-based and cumulative sensitivity forward models are implemented.
- Inversion algorithms include deterministic and stochastic methods.

Declaration of interest

None

Abbreviations

EC : electrical conductivity

ECa : apparent electrical conductivity

EMI : electromagnetic induction

ERT : electrical resistivity tomography

CS : cumulative sensitivity

LIN : low induction number approximation

FS : full solution, refers to the full solution of Maxwell's equation

Q : quadrature component (expressed as parts per thousand, ppt)

VCP : vertical co-planar

HCP : horizontal co-planar

PRP : perpendicular co-planar

Abstract

Frequency domain electromagnetic induction (EMI) methods have had a long history of qualitative mapping for environmental applications. More recently, the development of multi-coil and multi-frequency instruments is such that the focus has shifted to inverting data to obtain quantitative models of electrical conductivity. Whilst collection of EMI data is relatively straightforward, the inverse modeling is more complicated. Although several commercial and open-source inversion codes, exist, there is still a need for a user-friendly software that can bring EMI inversion to non-specialist audience. Here the open-source EMagPy software is presented as an intuitive approach to modeling EMI data. It comprises a graphical user (GUI) interface and a Python application programming interface (API). EMagPy implements both cumulative sensitivity and Maxwell based solution and can model/invert data for 1D and quasi-2D using either deterministic or probabilistic minimization methods. The EMagPy GUI has a logical 'tab-based' layout to lead the user through data importing, data filtering, inversion, and plotting of raw and inverted data. In addition, a dedicated forward modeling tab is presented to generate synthetic data. In this publication necessary considerations of EMI theory are described before its capabilities are presented through a series of environmental case studies. Specifically, the performance of cumulative sensitivity and Maxwell based forward models; the calibration of EMI data, a waterborne application and a time-lapse inversion are investigated. It is anticipated that despite the number of available EMI software, EMagPy offers a user-friendly tool suitable for novice and experienced practitioners alike, in addition to be useful for teaching purposes.

1 Introduction

1.1 Applications of electromagnetic induction

Ground-based frequency domain electromagnetic induction (EMI) methods use phenomena governed by Maxwell's equations to infer information about the electrical conductivity (EC) of the subsurface. As EC is the reciprocal of electrical resistivity, EMI methods can provide comparable information to electrical resistivity methods. However, given that they do not require direct coupling with the ground, they can, consequently, be more productive than standard electrical resistivity tomography (ERT) methods, particularly for surveying large areas. EMI measurements are typically expressed in terms of apparent electrical conductivity (ECa) and have a long history of being used to reveal spatial patterns of a number of hydrogeologically and agriculturally important properties and states; e.g. salinity (Corwin, 2008), water content (Corwin and Rhoades, 1984; Williams and Baker, 1982; Sherlock and McDonnell, 2003), soil texture (Triantafilis and Lesch, 2005) and soil organic matter (Huang et al., 2017). Furthermore, some studies have used repeated (i.e. time-lapse) measurements of ECa to also reveal temporal patterns, e.g. for soil water content estimation (Robinson et al., 2012; Martini et al., 2017).

In addition to ECa mapping, the development of multi-frequency and multi-coil instruments has enabled the possibility of inversion of EMI data to provide quantitative models of depth specific EC. For instance, by obtaining multiple EMI measurements with different sensitivity patterns, models of EC-ECa can be obtained. EMI inversions can be formulated as the minimization of the difference between measured and synthetic ECa values generated from a forward model. Most EMI inversion algorithms use a 1D forward model based on either the linear cumulative sensitivity (CS) forward model proposed by McNeill (1980) or non-linear full solution (FS) forward models based on Maxwell's equations (e.g. Wait, 1982; Frischknecht et al., 1987). Moreover, some EMI inversion programs, such as EM4Soil (Monteiro Santos, 2004) and the Aarhus Workbench (Auken et al., 2015), use lateral constraints to encourage laterally smoothed images using a 1D forward model; these methods are typically referred to as quasi-2D/3D inversion.

As with ECa mapping, EMI inversion has also been used in a wide range of applications, see Table 1. It is important to note differences in how EMI data are collected, processed and modeled. For instance, whether the EMI device is operated at ground level or an elevated level has implications for its sensitivity patterns. Furthermore, despite the availability of inversion software using FS forward models the CS forward model is still commonly used (e.g. Huang et al., 2016; Saey et al., 2016), despite its inherent simplifications. Lastly, there has also been interest in calibrating EMI measurements to account for factors relating to operation setup and permit the easier convergence of data. This is commonly done with either ERT or soil cores. Furthermore, it has been argued that calibration of EMI data is a prerequisite for inversion (e.g. Lavoue et al., 2011).

Table 1: Non-exhaustive list of environmental studies using inverted EMI data. HCP refers to horizontal co-planar, VCP refers to vertical co-planar and PRP refers to perpendicular orientation (all of which are defined in the text).

Reference	**Application**	**Survey acquisition**	**Inversion details**
Martinelli et al. (2008)	Chemical pollution	GEM-2 SLEM: six frequencies between 2575 and 47025 Hz	EM1DFMFW (Farquharson, 2003) with FS
Brosten et al. (2011)	Hydraulic conductivity	GEM-2, Height: 1 m HCP1.22 At 15 frequencies between 10 and 60 kHz	FEMIC with FS
von Hebel et al. (2014)	Structure	CMD Mini-Explorer Height: 0 m, VCP0.32, VCP0.71, VCP1.18, HCP0.32, HCP0.71, HCP1.18 At 30 kHz	SCE-UA with FS and CS
Davies et al. (2015)	Coastal salinity	DUALEM-421S Height: 0.2 m HCP1.0, PRP1.1, HCP2.0, PRP2.1, HCP4.0 PRP4.1 At 9 kHz	EM4Soil with FS
Jadoon et al. (2015)	Soil salinity	CMD Mini-Explorer Height: 0.05 m VCP0.32, VCP0.71, VCP1.18, HCP0.32, HCP0.71, HCP1.18 At 30 kHz	FS
Pederson et al. (2015)	Soil texture	DUALEM-421S Height: unknown HCP1.0, PRP1.1, HCP2.0, PRP2.1, HCP4.0 PRP4.1 At 9 kHz	Aarhus workbench
Shanahan et al. (2015)	Soil moisture	CMD Mini-Explorer Height: 0 m, VCP0.32, VCP0.71, VCP1.18, HCP0.32, HCP0.71, HCP1.18 At 30 kHz	McMC inversion with CS
Zare et al. (2015)	Soil salinity	DUALEM-421S Height: 0.2 m HCP1.0, PRP1.1, HCP2.0, PRP2.1, HCP4.0 PRP4.1 At 9kHz	EM4Soil with CS and FS
Christiansen et al. (2016)	Archaeology/ stratigraphy	DUALEM-421S, Height: ~0.2 m HCP1.0, HCP2.0, HCP4.0, PRP2.1, PRP1.1, PRP4.1 At 9 kHz	Aarhus Workbench with FS
Huang et al. (2016)	Soil moisture	DUALEM-421S Height: unknown	EM4Soil with CS

		HCP1.0, HCP2.0, HCP4.0, PRP2.1, PRP1.1, PRP4.1 At 9 kHz	
Saey et al. (2016)	Stratigraphy	DUALEM-421S Height: 0.16 m HCP1.0, HCP2.0, HCP4.0, PRP2.1, PRP1.1, PRP4.1 At 9 kHz	CS function
Frederiksen et al. (2017)	Stratigraphy	DUALEM-421S Height: ~0.285 m HCP1.0, HCP2.0, HCP4.0, PRP2.1, PRP1.1, PRP4.1 At 9 kHz	Aarhus Workbench with FS
Huang et al. (2017)	Soil organic carbon	DUAELM-21S Height: 0.075 m HCP1.1, HCP2.1 PRP1.1, PRP2.1 At 9 kHz	EM4Soil with FS and CS
Whalley et al. (2017)	Wheat root water uptake	CMD Mini-Explorer Height: 0 m, HCP/VCP s=0.32, 0.71, 1.18 m At 30 kHz	Gauss-Newton smoothed time-lapse with CS
Koganti et al. (2018)	Soil salinity	DUALEM-21S Height: 0.45 m HCP1.0, HCP2.0, PRP2.1, PRP1.1 At 9 kHz	EM4Soil with CS and FS
Von Hebel et al. (2019)	Stratigraphy	CMD Mini-Explorer Height: 0 m, VCP0.32, VCP0.71, VCP1.18, HCP0.32, HCP0.71, HCP1.18 At 30 kHz	SCE-UA with FS

There are several established commercial programs for processing and inverting frequency domain EMI data. Commercial programs include the Aarhus workbench (Auken et al., 2015), or EM4Soil (Monteiro Santos, 2004). In addition, several open source software codes exist, such as the Matlab-based open-source GUI for EMI data, FEMIC (Elwaseif et al., 2017), or the Python-based open-source codes SimPEG (Heagy et al., 2017) and pyGIMLI (Rücker et al. 2017). Open-source software has several benefits over commercial software, for instance it has better reproducibility, it is free and allows the user to interrogate the source code and, where necessary, adapt and customize for their own application. However, despite their availability, there is still a need for a comprehensive open-source software capable of bringing EMI inversion to a non-specialist audience. Given the increasing application of geophysics in multi-disciplinary projects, the need of a flexible and intuitive software for EMI inversion is a necessity.

In this work a Python-based open source EMI inversion software, EMagPy, is introduced. EmagPy has capabilities to generate synthetic data, filter and calibrate field data, and perform quasi-2D inversions. The inversion algorithms utilize either a Maxwell based FS forward model or the CS forward model, and provide the capability of obtaining smoothly and sharply varying models of EC. EmagPy provides a tab-based, user-friendly interface to that makes it accessible for novice users, making it ideal for teaching and training purposes. This manuscript provides a summary of the theoretical background to the software and highlights its capabilities through several case studies. Specifically, the case studies investigated are: (1) the performance of CS and FS solutions, (2) the impact of noise on the inversion results, (3) the impact of EMI calibration on inversion results, (4) EMI inversion for waterborne applications, and (5) time-lapse inversion of EMI data.

2 Material and methods

2.1 Theoretical background around on EMI

EMI devices operate by passing an alternating current through a transmitter coil to generate a primary electromagnetic field (H_P). This time-varying primary electromagnetic field interacts with the subsurface to induce eddy currents which in turn generate a secondary electromagnetic field (H_S). H_P and H_S are then recorded by the receiver coil, see Figure 1. The ratio of H_S and H_P is expressed as a complex number with an in-phase component (P) and an out-of-phase, or quadrature, component (Q). H_S/H_P is dependent on both the instrument set-up (e.g. operating frequency, coil separation and coil orientation) and subsurface conditions (e.g. magnetic, conductive and dielectric properties). At the frequencies used, dielectric properties can generally be ignored; furthermore, given that in most environments the subsurface can be considered as non-magnetic and the magnetic permeability of the subsurface is often assumed to be equal to that of free space (μ_0 = 1.257 x 10^{-8} H/m).

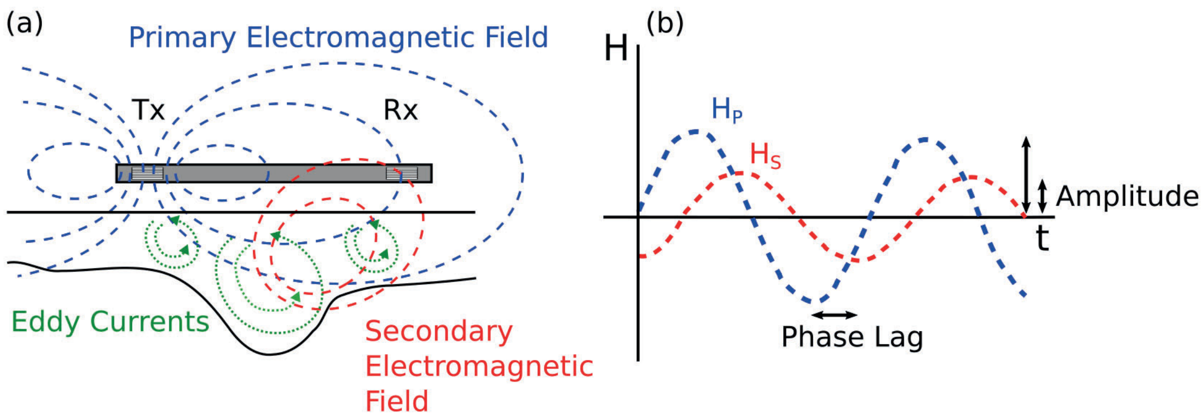

Figure 1: (a) Schematic of an EMI device with one transmitter coil (Tx) and one receiver coil (Rx). The transmitter emits a transient primary magnetic field (H_p) that induces eddy currents in the ground. These eddy currents generate a secondary electromagnetic field (H_s). Both

primary and secondary electromagnetic field are sensed by the receiver coil (b). From the complex ratio of their signals, information about the subsurface can be inferred.

For any given ground properties, the obtained H_S/H_P is dependent upon the separation distance between the transmitter and receiver coil, the operation frequency and the orientation of coils. The most used orientations are referred to as co-planar loops in which both the transmitter and receiver coils are orientated either horizontally (HCP) or vertically (VCP), with respect to ground. Another coil orientation is the perpendicular orientation (PRP) in which the transmitter and receiver loops are oriented at 90 degrees from each other. In addition, many devices are multi-coil or multi-frequency, meaning that measurements with different sensitivity patterns can be obtained by the same instrument, often simultaneously, and used for inverse modeling.

Most EMI instruments express their measured H_S/H_P values as values of apparent electrical conductivity, Eca. This term was introduced by McNeill (1980) to provide a more comprehensible measurement with the same units as EC, i.e., S/m. McNeill (1980) derived a linear relationship describing the Q value expected from a homogeneous subsurface electrical conductivity. The relationship therefore links the Q value of an assumed homogeneous subsurface to an Eca (i.e. the EC of a corresponding homogeneous ground). It is important to therefore note that it may not be valid in heterogeneous environments (see Callegary et al., 2007; Lavoue et al., 2010) and requires that (1) the device is operated on the ground, and (2) the induction number (β) is low (β << 1). The induction number is given by:

$$\beta = s\sqrt{\frac{2}{\omega\mu_0 EC}}, \qquad (1)$$

where σ is the conductivity of the ground, ω is the angular frequency ($2\pi f$) and s is the coil separation. The low induction number (LIN) approximation is described as:

$$EC_a = \frac{4}{\omega\mu_0 s^2}Q. \qquad (2)$$

It can be clearly seen from the expression that large frequencies and higher conductivity ground will violate the β << 1 specification proposed by McNeill (1980). Moreover, other more conservative β values of < 0.3 (Wait, 1962) and < 0.02 (Frischknecht, 1987) have also been provided for LIN conditions to be valid. It is also important to reiterate that the reliance of the LIN number approximation on a homogeneous subsurface also creates problems for its usage in heterogeneous environments and in cases where the device is operated above the ground. Nonetheless, it has been essential in advancing the EMI method.

2.2 Cumulative sensitivity forward model

In addition to the LIN approximation, McNeill (1980) provided functions to describe the relative contribution of materials below a specific depth to the overall Eca value when a device operates under LIN conditions. These CS functions assume that the sensitivity of the instrument is solely a function of the depth and coil separation and does not depend on the subsurface EC, or the device's operating frequency. The CS responses for VCP, HCP and PRP orientations are as follows:

$$R_{VCP}(z) = \sqrt{(4z^2+1)} - 2z, \qquad (3)$$

$$R_{HCP}(z) = \frac{1}{\sqrt{4z^2+1}}, \qquad (4)$$

$$R_{PRP}(z) = 1 - \frac{2z}{\sqrt{4z^2+1}}, \qquad (5)$$

Where z is the depth normalized by the coil separation, *s*. From equations 3 and 4 the sensitivities for different coil separations for the CMD Mini-Explorer and CMD Explorer (GF Instruments, Czech Republic), which can be operated in either VCP or HCP mode, can be calculated, see Figure 2. For instance, it can be seen that measurements made with coils in the VCP orientation are more sensitive to the shallow subsurface and measurements made in HCP orientation are sensitive to deeper depths. These functions are commonly used by manufacturers to provide information about the depth sensitivity of their instruments; i.e. the rule of thumb states VCP measurements have an effective depth of 0.75 times the coil separation and 1.5 times for HCP measurements.

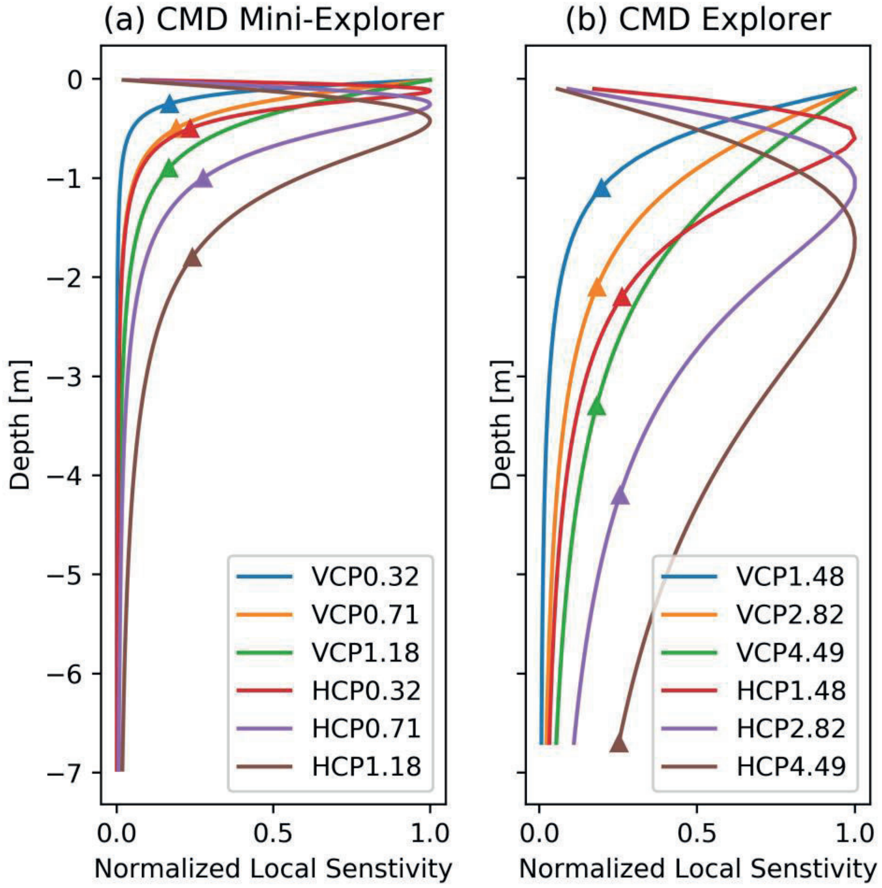

Figure 2: Normalized local sensitivity pattern of the coil configurations of two multi-coils instruments: (a) CMD Mini-Explorer and (b) CMD Explorer. Each coil configuration is first determined by its orientation (VCP/HCP here) and the Tx-Rx coil separation with units of meters. The triangles on each curve corresponds to the effective depth range supplied by the manufacturer.

As with the LIN approximation, the CS functions have been fundamental in advancing the EMI methods. Furthermore, despite the availability of inversion algorithms based on the FS forward model, the use of CS forward model in EMI applications is still common. This is largely due to their simplicity and speed in the inversion process compared to FS forward solutions. Furthermore, although, as with the LIN approximation, the CS forward model was developed for application when EMI devices are operated at ground level, several studies have used it to model the response of devices operated at some elevation by re-scaling the CS function (e.g. Andrade and Fisher, 2018).

2.3 Full Maxwell solution

In order to calculate a non-simplified response of the ground, in terms of H_S/H_P, a FS forward model must be used. The model used in EMagPy relies on the assumption that electromagnetic fields propagate only due to conduction currents, which is valid at low frequencies (< 10^5 Hz). The Maxwell-based full solution is provided by Wait (1982) and can be used to determine the response of an EMI instrument over a 1D layered earth consisting of N layers:

$$\left(\frac{H_S}{H_P}\right)_{VCP} = 1 - s^2 \int_0^\infty R_0 J_1(s\lambda)\lambda d\lambda, \tag{6}$$

$$\left(\frac{H_S}{H_P}\right)_{HCP} = 1 - s^3 \int_0^\infty R_0 J_0(s\lambda)\lambda^2 d\lambda, \tag{7}$$

$$\left(\frac{H_S}{H_P}\right)_{PRP} = 0 - s^3 \int_0^\infty R_0 J_1(s\lambda)\lambda^2 d\lambda, \tag{8}$$

where J_0 and J_1 are Bessel functions of zeroth and first orders, respectively, and R_0 is the reflection factor, which is dependent on the thickness and EC of each layer. The reflection factor is calculated at the interface of each layer, including between the air and the first layer. It can be obtained recursively from the infinite N^{th} layer, given that beyond N can be assumed homogeneous and therefore $R_{N+1} = 0$, and the following:

$$R_n = \frac{\frac{\Gamma_n - \Gamma_{n+1}}{\Gamma_n + \Gamma_{n+1}} + R_{n+1} e^{-2\Gamma_{n+1} h_{n+1}}}{1 + \frac{\Gamma_n - \Gamma_{n+1}}{\Gamma_n + \Gamma_{n+1}} e^{-2\Gamma_{n+1} h_{n+1}}}, \tag{9}$$

where $\Gamma_n = \sqrt{(\lambda^2 + i\omega\mu_0 EC_n)}$, and h_n and EC_n are the thickness and the EC of the n^{th} layer. R_0 is obtained by assuming the EC of layer 0 is 0 S/m to reflect the air. The integrals in equations 6, 7 and 8 represent the Hankel transform and can be calculated by linear filtering (Guptasarma and Singh 1997; Anderson 1979). As noted, most devices provide measurements as an ECa, therefore in order to use the FS forward model the obtained Q values from equations 6, 7 and 8 need to be converted to an ECa value. This translation is important, as discussed below.

2.4 Comparing ECa values and forward models

Although the LIN approximation (equation 2) offers a comprehensible unit to represent the subsurface EC, several authors have developed methods to provide more representative ECa values, especially when LIN assumptions are not met. For instance, although most manufactures state that their EMI devices operate under LIN conditions and use the LIN approximation to obtain ECa values, Beamish (2011) demonstrated that LIN assumptions are only valid at low EC values (< 12 mS/m). Hanssens et al. (2019) provide an overview of various methods; typically methods focus on just the Q component (e.g. Andrade et al., 2016; von Hebel et al., 2019) or use both the P and Q components (e.g. Huang and Won, 2000; Guillemoteau et al. (2015) to obtain ECa values more representative of the subsurface.

Because of the generally weakly magnetic subsurface in environmental cases, and the characteristic instability of P measurements (Lavoue et al., 2011), in EMagPy a method akin to van der Kruk et al. (2000), Andrade et al. (2016), and von Hebel et al. (2019) is used to compute a more representative ECa. This is done by minimizing the absolute difference between an observed Q value and a Q value for an equivalent homogeneous subsurface conductivity:

$$min(|Q_{target} - Q_{homo}|). \tag{10}$$

The ECa value obtained from this method therefore closely matches the EC of a homogeneous subsurface. As this optimization can be subject to localized minima, in EMagPy it is initialized with the LIN approximation, and although this may be ambiguous at large conductivities (see Hanssens et al., 2019), in the majority of cases the ground EC is sufficiently low to not cause problems.

Although this method provides a more representative ECa, the key importance of inverting EMI data using the FS forward model is that modeled ECa are obtained from Q using the same method used to convert Q to ECa in EMI devices. For instance, although in most cases devices use the LIN approximation, some EMI devices use a manufacturer calibration. For example, GF Instruments use a manufacturer calibration based on a linear fit through the Q values obtained at two sites of known subsurface EC. In addition, different calibrations exist for when their devices are operated at ground level and 1 m, such that measurements made at 1 m elevation are more representative of the true ground EC. This would mean, for instance, that if ECa values using the GF Instruments 1 m calibration were converted to Q using the LIN approximation they would be significantly higher than actually measured.

Furthermore, although the CS is also based on LIN assumptions, the ECa values obtained from the CS forward model differ, in some cases, from the ECa obtained from LIN approximation and Q values measured in the field. This means that under certain scenarios use of the CS forward model could result in erroneous inversion. In this work a distinction between an ECa value from equation 2 (LIN-ECa), an ECa value from equation 10 (FS_{EQ}-ECa) and from the CS forward models (equations 3, 4 and 5) (CS-ECa) is made, see Fig. 3.

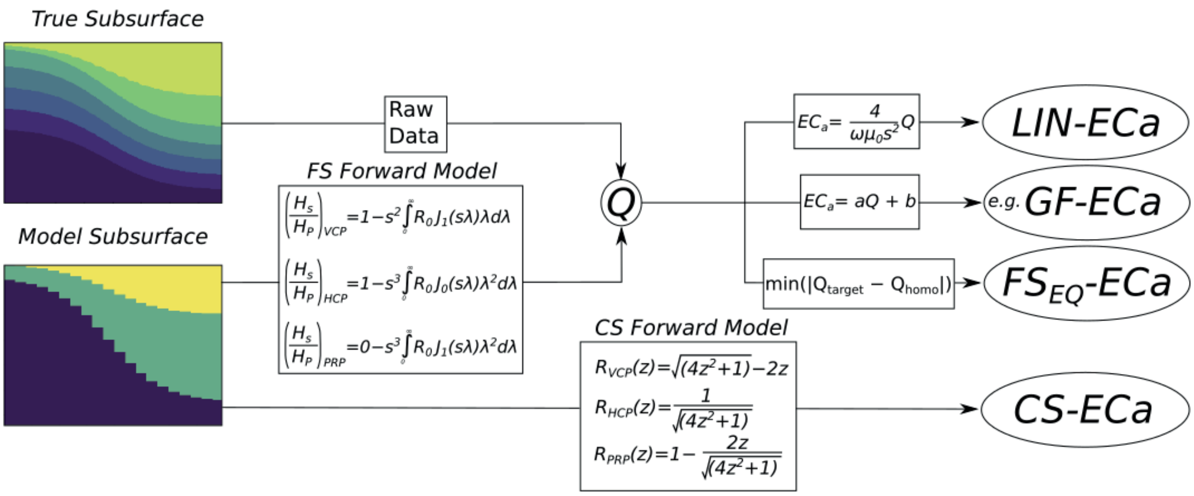

Figure 3: The different routes for obtaining ECa values. For field cases all devices obtain a Q value which is typically transformed into an ECa using either the LIN-ECa or some other manufacturer calibration (e.g. the GF instruments linear calibration). Some authors (e.g. von Hebel et al. 2019) opt to convert their field obtained Q values using a minimizing approach (FS_{EQ}-ECa). For modeled cases there are two principle routes to obtain ECa values from a model subsurface: (1) Q values may be calculated from the FS forward model, they would then typically be converted to LIN-ECa or FS_{EQ}-ECa, and (2) CS-ECa values can be obtained directly using the CS forward model.

To highlight the distinctions of ECa values defined here, and hence stress the importance of their difference, they can be computed for a variety of synthetic cases. In Figure 4, FS_{EQ}-ECa, LIN-ECa and CS-ECa are calculated for the device specifications of the largest coil separation (4.49 m) of the CMD Explorer operated in VCP mode above homogeneous and heterogeneous subsurfaces, at ground level and at 1 m elevation. For the homogeneous case, data are generated for subsurface EC of 1 to 100 mS/m in 1 mS/m increments, the heterogeneous case data is generated for a two layer model with a layer 1 thickness of 0.5 m, an upper layer EC of 1 to 100 mS/m in 1 m/Sm increments and a constant lower layer EC of 50 mS/m.

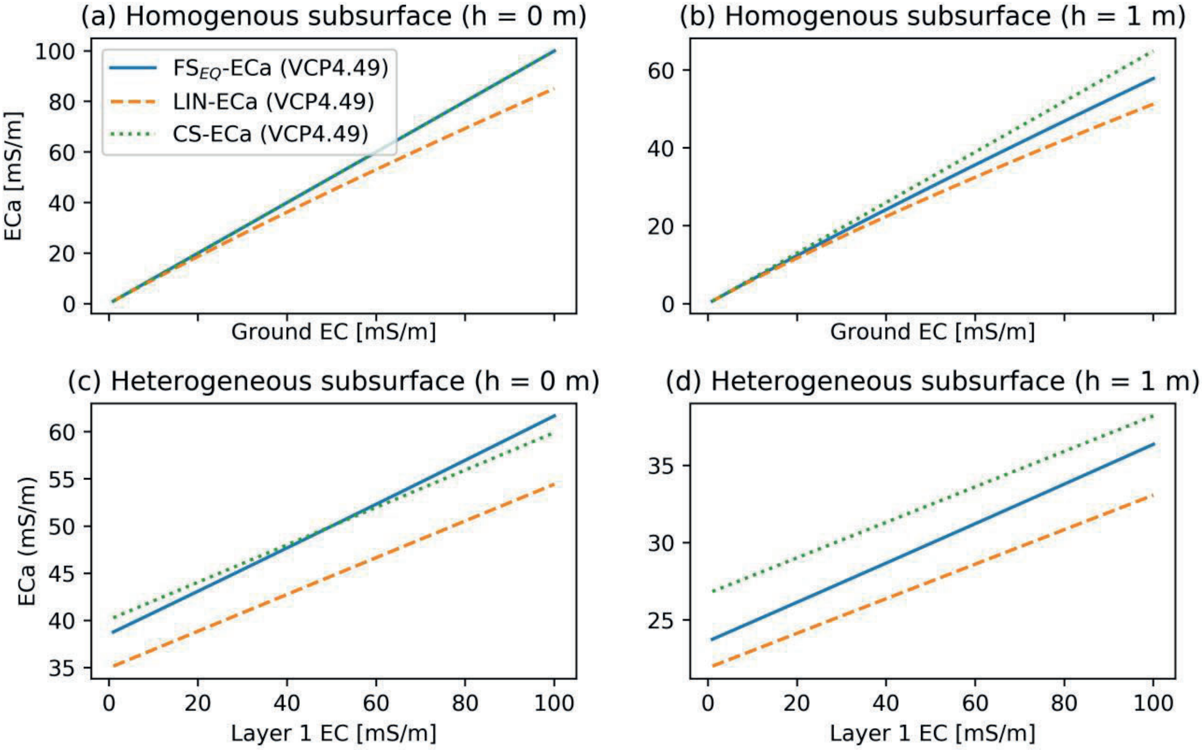

Figure 4: Differences between CS-ECa, FS$_{EQ}$-ECa and LIN-ECa for a homogeneous and a heterogeneous case. (a) shows the differences over a homogeneous medium with increasing EC, (b) shows the differences over an increasing homogeneous medium when the device is operated at 1 m, (c) shows the differences over a heterogeneous medium with a fixed layer 1 thickness of 0.5 m and a fixed EC of 50 mS/m, and (d) shows the differences over a heterogeneous medium with a fixed layer 1 thickness of 0.5 m and a fixed EC of 50 mS/m when the device is operated at 1 m elevation. In all figures h *is the device height above ground level.*

Firstly, it can be seen from Fig. 4a that for a homogeneous subsurface EC when the device at ground level FS$_{EQ}$-ECa and CS-ECa values lie on a 1:1 line, whereas the LIN-ECa deviates from this line at higher EC values. In comparison, when the device is operated at 1 m elevation (Fig. 4b) FS$_{EQ}$-ECa, LIN-ECa CS-ECa all show increasing deviation at higher conductivities, with the FS$_{EQ}$-ECa being intermediate between the higher CS-ECa and the lower LIN-ECa. Furthermore, these values are broadly comparable for low conductivities (< 20 mS/m), for the ground level and 1 m elevation cases. When the device is operated at ground level (Fig. 4c), for the heterogeneous case, the LIN-ECa is significantly lower than the other two values. Furthermore, the FS$_{EQ}$-ECa and CS-ECa match when the upper layer conductivity is 50 mS/m (i.e. homogeneous subsurface). When the device is operated at 1 m elevation (Fig. 4d) for the heterogeneous case all ECa values differ from each other across the layer 1 conductivity range.

These observations demonstrate that under certain conditions the CS function may be inappropriate to model with LIN-ECa values obtained from the field, e.g. when the subsurface is strongly heterogeneous. Furthermore, it can also be noted that FS_{EQ}-ECa is perhaps better suited to modeling than the CS function and may perform reasonably in environments where subsurface EC is both low and of small variability. Moreover, if FS_{EQ}-ECa is taken as the most accurate representation of the subsurface EC, it can be seen that LIN-ECa underestimates the subsurface EC in the case of higher EC values and heterogeneous environments. However, as noted above, so long as the translation between Q and ECa is consistent for the EMI device and FS forward model, the derivation of ECa using this method is not a requisite for accurate inversion.

2.5 Calibration of EMI data

In addition to considering ECa values, it is important to note that in many cases EMI devices are only seen to provide qualitative measurements of conductivity because of instrument calibration difficulties (Triantafilis et al. 2000; Sudduth et al. 2001; Abdu et al. 2007; Gebbers et al. 2009; Nüsch et al. 2010). For instance, external influences such as presence of the operator, zero-leveling procedures or field set up can influence the measurements significantly. Therefore, in order to permit quantitative modeling of EMI data several authors have advocated for the need of data calibration (e.g. Lavoue et al., 2009; von Hebel et al., 2014). Proposed calibration methods have included collection of intrusive soil samples (e.g. Triantafilis et al. 2000; and Moghadas et al., 2012), use of ERT (e.g. Lavoue et al., 2010; von Hebel et al., 2014) or use of measurements made at multiple elevations (e.g. Tan et al., 2019).

In this work the method using ERT is implemented, whereby depth-specific models of electrical resistivity are used to calculate a forward EMI model response which is then paired with a set of EMI measurements made along the ERT transect. Although it is possible to invert ERT data with several inversion programs, the calibration implementation in EMagPy can directly use ERT models produced by the sister code, ResIPy (https://gitlab.com/hkex/pyr2; Blanchy et al., 2020). Clearly, there is an implicit assumption here that the ERT-derived electrical conductivities are true values, and that the footprint of EMI and ERT measurements does not differ significantly.

2.6 Inversions routines

2.6.1 Data and model misfit

In EMagPy the inverse problem can be solved using the CS or FS forward model solutions, in addition the problem can be solved to produce both sharply and smoothly varying models of conductivity. The sharp inversion solves the inverse problem with both conductivities and depths as parameters, whereas the smooth inversion uses fixed depths and solves only for conductivities. In both cases the data misfit is defined as the difference between observed values and predicted values from the forward model solutions. As the smooth inversion typically produces a model containing more EC values than measurements it requires a model misfit term, which determines the smoothness of neighboring layers. In comparison, the sharp inversion, although a model misfit term can be used, the inverse problem is generally set such that the problem is under-determined, i.e. the number of parameters (depths and conductivities) is less than the number of measurements. The total misfit is given by:

$$\Phi = \Phi_d + \alpha\Phi_m, \tag{10}$$

where Φ_d is the data misfit, Φ_m is the model misfit and α is a smoothing parameter determining the influence of Φ_m on the total misfit, i.e. ordinarily this would be set to 0 for sharp cases. The inversion problem can be solved by minimizing either the L1 or the L2 norm cost functions for each 1D profile. The data misfit for both norms are obtained by:

$$\Phi_d = \frac{1}{N}\sum_{i=1}^{N}\left|d_i - f_i(m)\right|, \tag{11}$$

$$\Phi_d = \frac{1}{N}\sum_{i=1}^{N}\left(d_i - f_i(m)\right)^2, \tag{12}$$

where N is the number of coil configurations per profile, d is the observed values and $f(m)$ is the predicted values from the forward model with parameter set, m. Similarly, the model misfits for L1 and L2 norms, respectively, are obtained by:

$$\Phi_m = \frac{1}{M}\sum_{j=1}^{M-1}\left|EC_j - EC_{j+1}\right|, \tag{13}$$

$$\Phi_m = \frac{1}{M}\sum_{j=1}^{M-1}\left(EC_j - EC_{j+1}\right)^2, \tag{14}$$

where M is the number of layers in the model and EC_j is the conductivity of layer j.

2.6.2 Optimization methods

In EMagPy, the total misfit can be minimized using three groups of methods (see Table 2): using either (1) a Gauss-Newton method, (2) optimization from the scipy package (Virtanen et al., 2020), or (3) McMC optimization from the spotpy package (Houska et al., 2015). The Gauss-Newton implementation is straightforward; it is exclusively for the CS function as the Jacobian (sensitivity) matrix can be obtained easily. This implementation requires fixed depths and requires a large α value. As the Jacobian matrix for the CS function does not depend on the layer conductivity, the solution is reached in one iteration. It is therefore well suited for quick inversions of smooth solutions and has the added benefit that it easily enables time-lapse inversion (see Whalley et al., 2017).

Table 2: Minimization methods employed within EMagPy.

Minimization method	Description	Implemented features	Package used
Gauss-Newton	Gradient based method.	CS forward model, L2 data and model misfit.	-
Nelder-Mead	Simplex heuristic search method.	CS and FS forward model, L1 and L2 data and model misfit.	scipy
L-BFGS-B	Approximation of BFGS method, with bounds. This method uses an estimate of the inverse Hessian matrix.	CS and FS forward model, L1 and L2 data and model misfit.	scipy
Conjugate Gradient	Gradient method for non-linear problems.	CS and FS forward model, L1 and L2 data and model misfit.	scipy
SCE-UA	Shuffled Complex Evolution Algorithm McMC based method.	CS and FS forward model, L1 and L2 data and model misfit.	*spotpy*
DREAM	Differential Evolution Adaptive Metropolis Algorithm McMC based method.	CS and FS forward model, L1 and L2 data and model misfit.	*spotpy*
ROPE	Robust Parameter Estimation McMC method	CS and FS forward model, L1 and L2 data and model misfit.	*spotpy*

Through the optimize function from scipy, EMagPy can minimise equation 10 using the Nelder-Mead (Nelder and Mead, 1965), L-BFGS-B (Byrd et al., 1995) or conjugate gradient (Fletcher and Reeves, 1964) algorithms. However, it is important to note that broader range of algorithms exist though the scipy package and can be implemented if needed. These methods can be used for both the CS and FS forward models and are adapted to both smooth and sharp inversions. Their implementation is based on the function `scipy.optimize.minimize()` from the *scipy* python package that is used to minimize the objective function. Each method has its own convergence criteria (see *scipy* documentation)

The McMC-based approach also minimizes an objective function but relies on different sampling approaches to find a solution. This implementation is based on the Python *spotpy* package (Houska et al., 2015) that provides several solvers for parameter optimization such as SCE-UA (Duan et al., 1994), DREAM (Vrugt and Ter Braak, 2011) or ROPE (Bardossy et al., 2008). One advantage of this approach is that it produces posterior distribution of the parameters from which a model uncertainty can be estimated (Figure 5). In EMagPy, this posterior distribution is based on the 10% best sample (i.e. the lowest total misfit) and the error for each parameter is estimated using the standard deviation of this posterior distribution. Although this method was primarily implemented to obtain sharp models of EC, it can also be used for smooth models.

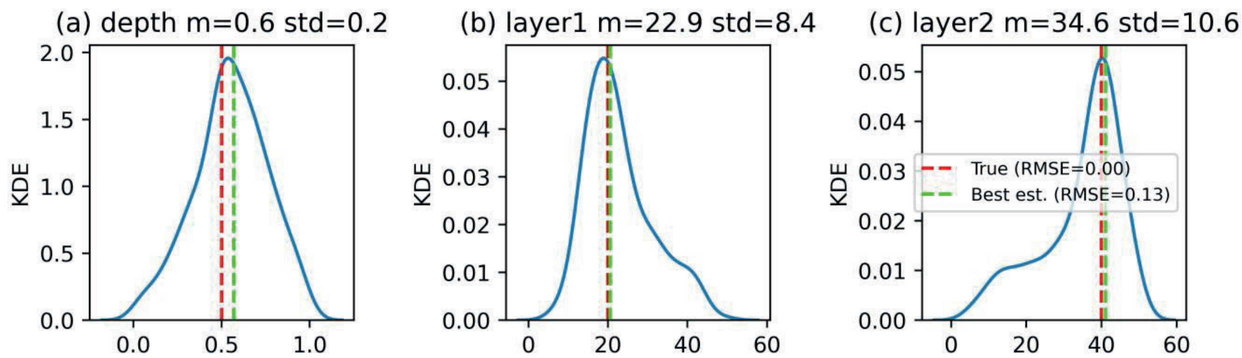

Figure 5: Example of a two layers, one varying depth model inverted using the McMC solver. Each subplot shows the posterior distribution of the parameters after sampling (3000 samples, 1 chain) for (a) the depth, (b) the EC of layer 1 and (c) the EC of layer 2. m *is the mean and* std *is the standard deviation of the distribution (meters for depth and mS/m for layer1 and layer2). The red dashed line represent the true value while the green dashed line represent the best estimate (the one with the lowest misfit).*

The quality of the inversion can be assessed visually by plotting the predicted ECa values from the inverted model and the observed ECa for each profile using either `showMisfit()` or `showOne2one()` methods. It is also possible to directly plot the root-mean-square error for each profile on top of the inverted section using `showResults(rmse=True)`. This makes it easy to quickly identify how suitable models are for explaining the different EMI observations.

2.7 EMagPy capabilities

EMagPy has been designed to provide both a Python application programming interface (API) and a graphical user interface (GUI). The Python API can be used in Python scripts or in Jupyter notebooks and enables automated tasks. The GUI provides an intuitive interface for the inversion and modeling of multiple datasets.

In EMagPy, the code is structured around two main classes, a Survey and a Problem class. The Survey class that contains information related to the survey (such as the ECa values and their locations) and several display functions. Whereas the `Problem` class handles the forward and the inverse modeling and displays the results. Multiple surveys can be imported, to allow for time-lapse inversion. If geographical information (e.g. x and y coordinates) is available, map views can be used to show the apparent or inverted data. Figure 5 summarizes the capabilities of EMagPy. A more exhaustive list of API methods can be found in Appendix A.

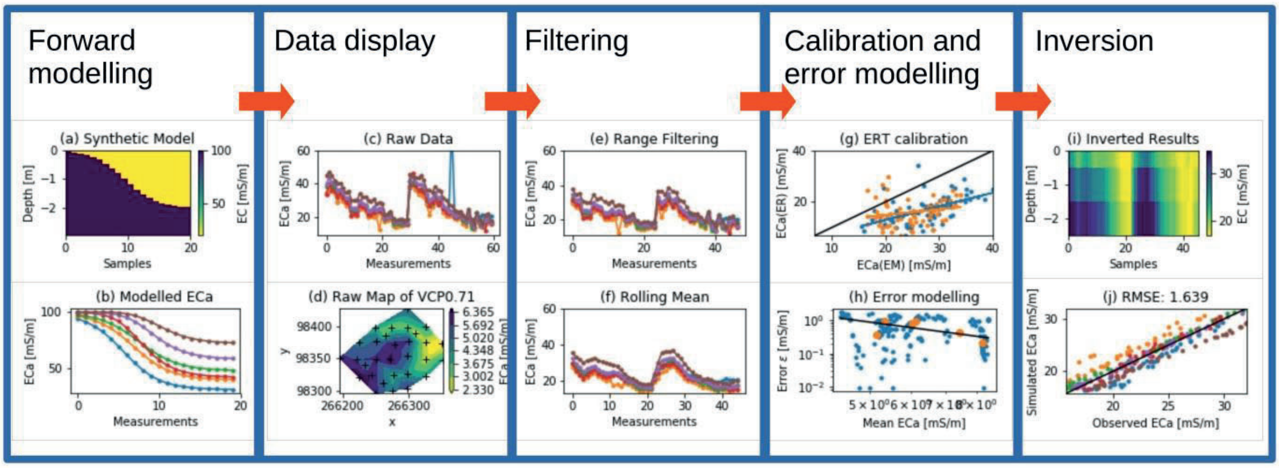

Figure 6: Capabilities of EMagPy workflow. Given a defined depth-specific EC model (a), synthetic apparent ECa can be modeled (b). Alternatively, field measurements can be imported and displayed as line plot (c) or map (d). Range filtering (e) and rolling mean (f) are among the options available to filter the measurements. If an ERT transect has been collected, a quantitative calibration of the measurement can be done (g). If cross-over points were collected, an error model can be derived (h). (g) shows the inverted data and (j) how well the modeled ECa fits the observed ECa.

Along with a pure Python API, EMagPy offers a graphical user interface (GUI) composed of several tabs exploiting the capabilities of the API (Figure 6). The purpose of the interface is to provide a standalone intuitive user-friendly tool.

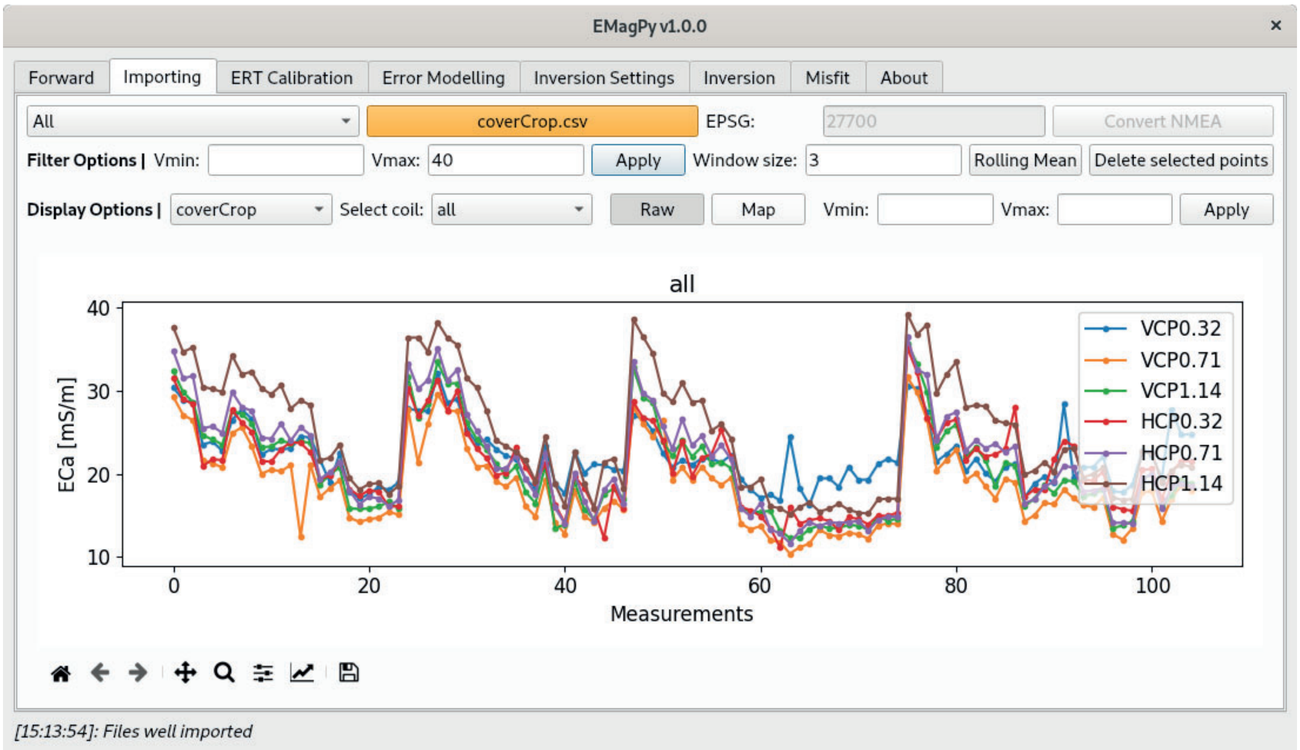

Figure 7: EMagPy graphical user interface is composed of several tabs that guide the user through the EMI processing workflow. At first the measurements are imported and filtered or alternatively they can be synthetically generated in the 'Forward' tab. Then an ERT calibration (if available) can be performed and an error model can be fitted if there are cross-over points. Then in the "Inversion Settings" tab the number of layers and their depths is defined as well as other inversion options. The inversion results are displayed in the 'Inversion' tab and the 'Post-processing' tab helps to assess the quality of the inversion.

3 Case studies

The following case studies presented here are included to demonstrate the ability of EMagPy for forward modeling and inversion. In addition, the Python code of the case studies presented below is available on the Gitlab repository of the project for anyone to reproduce (https://gitlab.com/hkex/emagpy/-/blob/master/jupyter-notebook/em-paper.ipynb).

3.1 Impact of different forward models on inversion

The first case demonstrates EMagPy's forward modeling capabilities and investigates the difference between FS and CS forward models for a heterogeneous subsurface. Data were generated from the synthetic model displayed in Fig. 5, i.e. a two layer model comprising an upper layer with an EC of 20 mS/m and a lower layer with an EC of 100 mS/m. Data were generated in terms of LIN-ECa using the FS forward model for the instrument properties of the CMD-Explorer operated at ground level and 1 m before being inverted using either the FS forward model or the CS forward model. It can be seen for both 0 m and 1 m elevations the FS results match the synthetic model in terms of depth and EC. In comparison, although the CS results pick up the depth reasonably well for the 0 m elevation case, the EC values of the second layer are not well resolved.

```
# parameters for the synthetic model
nlayer = 2 # number of layers
npos = 20 # number of positions/sampling locations
conds = np.ones((npos, nlayer))*[10, 50] # EC in mS/m
x = np.linspace(0.1, 2, npos)[:,None]
depths = 0 + 2/(1+np.exp(-4*(x-1))) # depth of model

# defines coils configuration, frequency and height above the ground
coils0 = ['VCP1.48f10000h0', 'VCP2.82f10000h0', 'VCP4.49f10000h0',
          'HCP1.48f10000h0', 'HCP2.82f10000h0', 'HCP4.49f10000h0']
coils1 = ['VCP1.48f10000h1', 'VCP2.82f10000h1', 'VCP4.49f10000h1',
          'HCP1.48f10000h1', 'HCP2.82f10000h1', 'HCP4.49f10000h1']

# forward modeling
ks = []
for i, coils in enumerate([coils0, coils1, coils0, coils1]):
    k = Problem()
    k.setModels([depths], [conds])
    _ = k.forward(forwardModel='FSeq', coils=coils, noise=0)
    ks.append(k)
k.showResults() # display original model
k.show() # display ECa computed from forward modeling

for k, fm in zip(ks, ['FSeq','FSeq','CS','CS']):
    k.setInit(depths0=[0.5], fixedDepths=[False],
              conds0=[20, 20], fixedConds=[False, False]) # set initial values
    # invert using ROPE solver (RObust Parameter Estimation)
    k.invert(forwardModel=fm, method='ROPE', regularization='l1',
             bnds=[(0.01, 3), (0, 80), (0, 80)], rep=1000, njobs=-1)
```

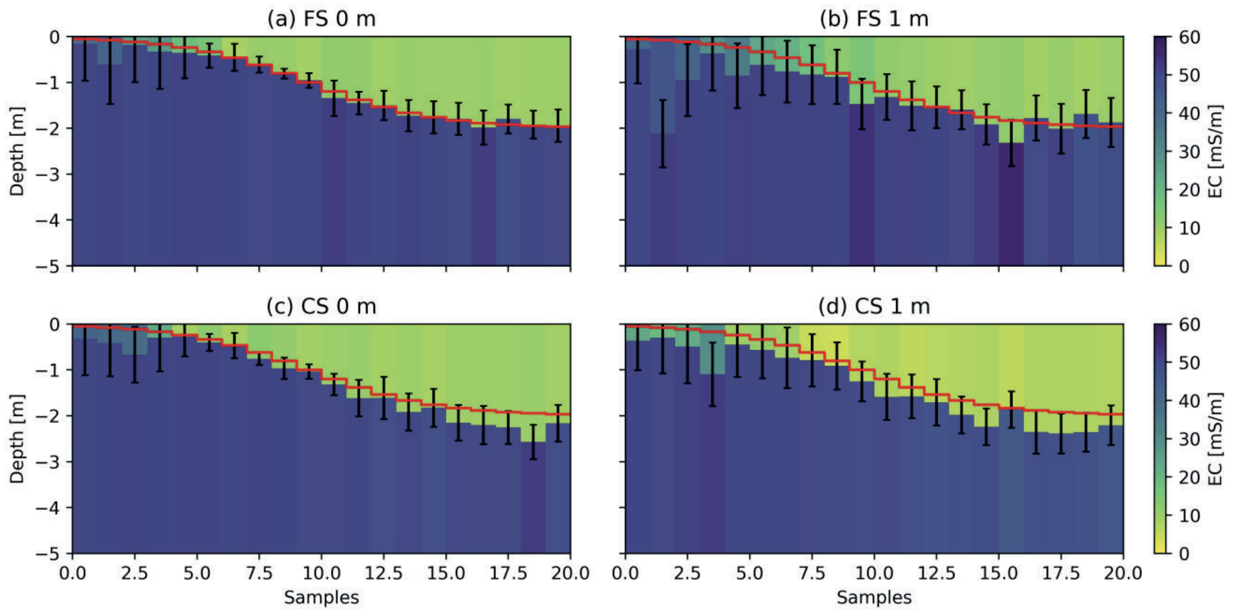

Figure 8: Inverted model with (a) FS_{EQ} at 0 m, (b) FS_{EQ} at 1 m, (c) CS at 0 m, (d) CS at 1 m. The red lines denote the true interface between the two layers of 20 and 100 mS/m from top to bottom. The error bars show the standard deviation of the posterior distribution (based on the 10% best sample).

3.2 Impact of measurement noise on inversion

To investigate the influence of measurement noise on the inversion when the device is operated at ground level and at 1 m, data were generated for a two layer model with an undulating interface. The upper layer EC was set at 20 mS/m and the lower layer EC was set at 100 mS/m, synthetic data were then generated using the FS forward model and corrupted with 2% Gaussian noise. Data with, and without noise, were then inverted. It was observed that in the noise-free cases, when the device is at 0 m and 1 m, the synthetic model is resolved relatively well (Figure 8). This is also true for the data containing noise when operated at ground level but when elevated at 1 m elevation the inversion performs much poorer.

```
# parameters for the synthetic model
nlayer = 2 # number of layers
npos = 20 # number of sampling locations
conds = np.ones((npos, nlayer))*[20, 100]
x = np.linspace(0.1, 2, npos)[:,None]
depths = 0.65 + 0.15* np.sin(x*np.pi*2)
coils0 = ['VCP1.48f10000h0', 'VCP2.82f10000h0', 'VCP4.49f10000h0',
```

```
           'HCP1.48f10000h0', 'HCP2.82f10000h0', 'HCP4.49f10000h0']
coils1 = ['VCP1.48f10000h1', 'VCP2.82f10000h1', 'VCP4.49f10000h1',
           'HCP1.48f10000h1', 'HCP2.82f10000h1', 'HCP4.49f10000h1']
coils = [coils0, coils0, coils1, coils1]
noises = [0, 0.05, 0, 0.05]
ks = []
# generate ECa using forward model
for i in range(4):
    k = Problem()
    k.setModels([depths], [conds])
    _ = k.forward(forwardModel='FSeq', coils=coils[i], noise=noises[i])
    ks.append(k)

# invert
for k in ks:
    k.setInit(depths0=np.array([0.5]), fixedDepths=[False])
    k.invert(forwardModel='FSeq', method='ROPE', regularization='l1',
             bnds=[(0.05, 2.5), (5, 150), (5, 150)], rep=1000, njobs=-1)
```

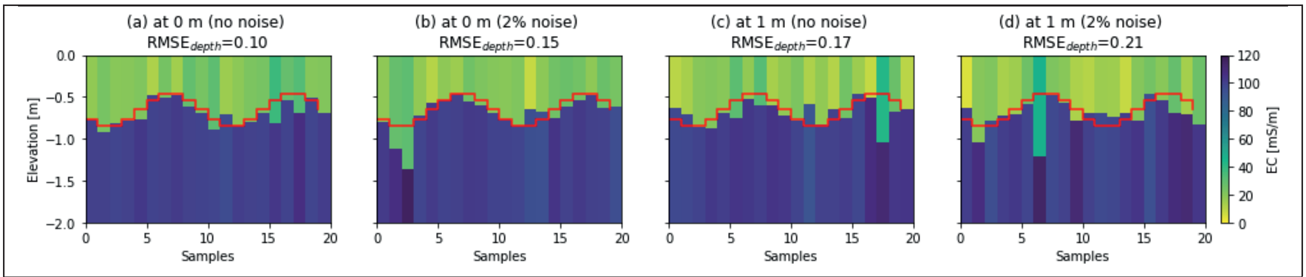

Figure 9: All inversions are performed with the ROPE solver on a two-layer model with a varying depth. (a) Inversion with 0% noise with device on the ground. (b) Inversion with 2% noise on the ground. (c) Inversion with 0% noise at 1 m above the ground (d) Inversion with 2% noise at 1 m above the ground. The red line represents the true interface between the two layers.

3.3 ERT Calibration of EMI data

In this case study, data collected from a riparian wetland using the CMD-Explorer are used to highlight how calibration of data can improve inversion performance. The riparian wetland is characterized by peat and underlying gravel and revealing the depth of the peat is of interest in characterizing the hydrology of the site (see Newel et al., 2015). ERT data were collected with a Syscal Pro 96 (Iris Instruments, Orleans, France) with 96 electrodes spaced of 0.5 m using a dipole-dipole sequences comprising 2342 measurements. An inverted EC section was obtained using ResIPy (Blanchy et al., 2020). It can clearly be seen that when not calibrated (Fig. 8a), the inversion fails to reveal the pattern of the peat, however when calibrated (Fig. 8b) the peat depth and EC more closely resembles the ERT image (Fig. 8c).

```
fnameEC = datadir + 'boxford-calib/eri_ec.csv'
fnameECa = datadir + 'boxford-calib/eca_calibration2.csv'

# non calibrated
k1 = Problem()
k1.createSurvey(fnameECa)
k1.show()
k1.setInit(depths0=np.arange(0.05, 3, 0.05))
k1.invert(alpha=0.001,njobs=-1)

# ERT calibrated
k2 = Problem()
k2.createSurvey(fnameECa)
k2.calibrate(fnameECa, fnameEC, forwardModel='FSeq') # plot calibration
k2.calibrate(fnameECa, fnameEC, forwardModel='FSeq', apply=True) # apply the
calibration
k2.setInit(depths0=np.arange(0.05, 3, 0.05))
k2.invert(alpha=0.001,njobs=-1)
```

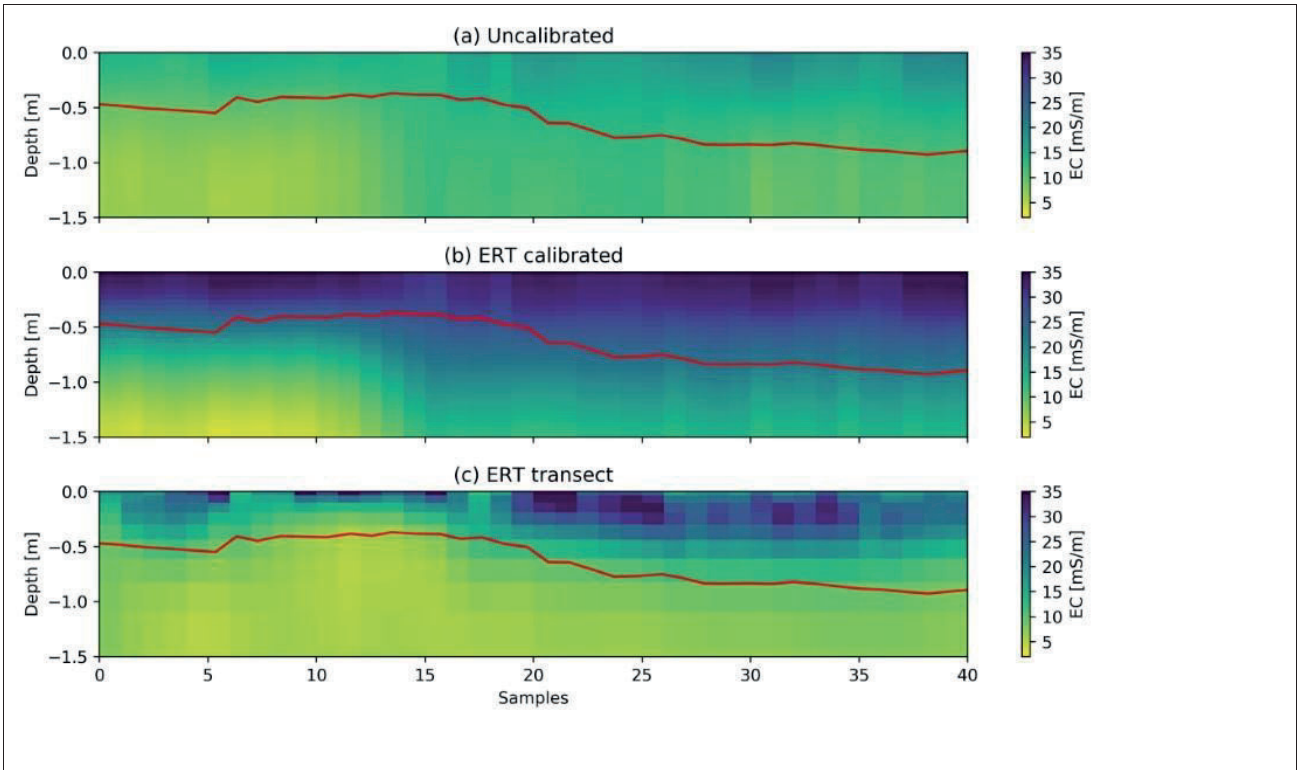

Figure 10: Smoothly inverted non-calibrated (a) and calibrated (b) EMI data with the corresponding ERT inversion (c). The red line shows the true depth of the peat intrusive penetration measurements.

3.4 Including prior knowledge

EMagPy also permits the fixing of initial model parameters within the inversion. This may be useful if *a priori* knowledge is available, i.e. structural information obtained from intrusive or geophysical methods. Moreover, in such cases, smoothing is automatically prevented between layers with fixed and non-fixed conductivities. Prior information is available in the case of aquatic surveys where the depth and EC of the river can easily be measured. In this case, data was collected from a site is characterized by zones of groundwater up-welling, which have been shown previously to be sites of nitrate loading from legacy agricultural pollution (Binley et al., 2013). EMI data were collected using a CMD-Explorer mounted on an inflatable kayak, 0.4 m above the surface of the water using both HCP and VCP orientations. River depths were determined from a pressure logger (see Binley et al., 2013) and river EC was determined with an EC meter. The river depth varied from 0.14 to 1.18 m along the survey and the river water EC was 48 mS/m. On Figure 10, ECa values from the river-borne survey are inverted with fixed river depth and fixed EC for the top layer corresponding to river water. It can be seen that the EC of the riverbed is higher on the upstream side; this is in broad agreement with hydraulic head data presented in Binley et al. (2013) and can interpreted to be a result of up-welling of the more conductive groundwater.

```
k = Problem()
k.createSurvey(datadir + 'leith/leith_dataset.csv')
depths = k.surveys[0].df['depth'].values # measured water depths
# setting initial model with top layer (the river) with fixed EC of 48 mS/m
(measured)
k.setInit(depths0=depths[:,None], conds0=[48, 20], fixedConds=[True, False])
k.invert(njobs=-1, beta=0.1) # beta > 0 will cause lateral smoothing
```

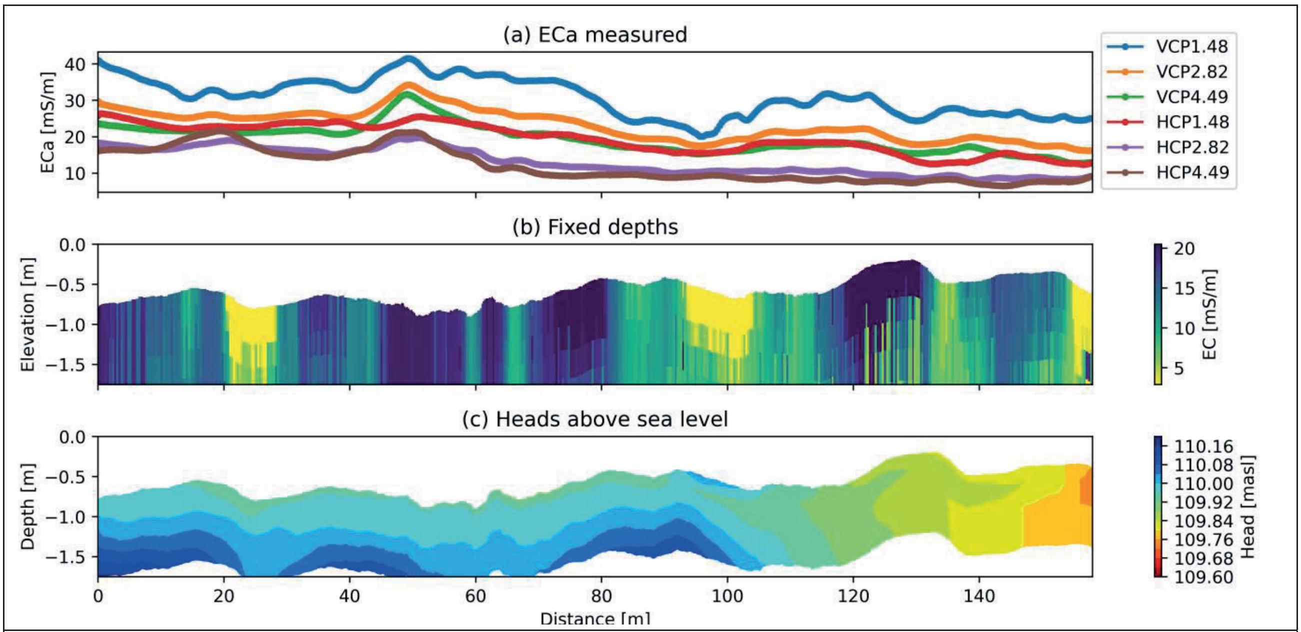

Figure 11: (a) ECa values measured from a CMD-Explorer on a boat along the river. (b) Inverted EC values given a fixed depth and a fixed EC of the top layer representing the river water (only the river bed conductivity is shown). (c) Hydraulic heads in the river bed from Binley et al. (2013). Upstream is at 0 m and downstream at 160 m distance.

3.5 Time-lapse field application

In the last case study, the capabilities to perform time-lapse EMI inversion are shown. EMI measurements can be used as a proxy for soil moisture (e.g., Whalley et al., 2017). Using a pedophysical relationship (Laloy et al, 2010), the change in inverted EC beneath different wheat varieties can be linked to change in soil moisture. This method provides to crop breeders high-throughput non-invasive below-ground information that can be important for selecting resilient varieties. In this scenario, EMagPy can invert for the change in conductivity using the Gauss-Newton solver using the method described in Appendix 1 of Whalley et al. (2017). In this experiment ECa measurements were collected using a CMD Mini-Explorer on different winter wheat plots during the growth season. At the same time, soil moisture measurements were taken using neutron probe as ground truth. Note that all ECa values were calibrated using an ERT array and temperature corrected. Figure 10a shows the inverted EC In March 2017 while Figure 10e shows the volumetric water content measured by neutron probe. Figures 10b, 10c and 10d show the change in EC, in mS/m, from this the EC of 10a, and Figures 10f, 10g and 10h show the changes in water content, in relation to Figure 10d. Larger decreases in EC are observed at deeper depths through the growing season and can be attributed to crop growth and water uptake.

```
# inversion of change
fnames = [
        datadir + 'timelapse-wheat/2017-03-16.csv',
        datadir + 'timelapse-wheat/2017-04-03.csv',
        datadir + 'timelapse-wheat/2017-04-27.csv',
        datadir + 'timelapse-wheat/2017-05-16.csv']
k = Problem()
k.createTimeLapseSurvey(fnames) # import all surveys
k.setInit(depths0=np.linspace(0.1, 2, 10)) # smooth multiple fixed depths model
k.computeApparentChange() # compute change in ECa compared to first survey
k.invert(forwardModel='CSgn', alpha=0.07) # Gauss-Newton routine
```

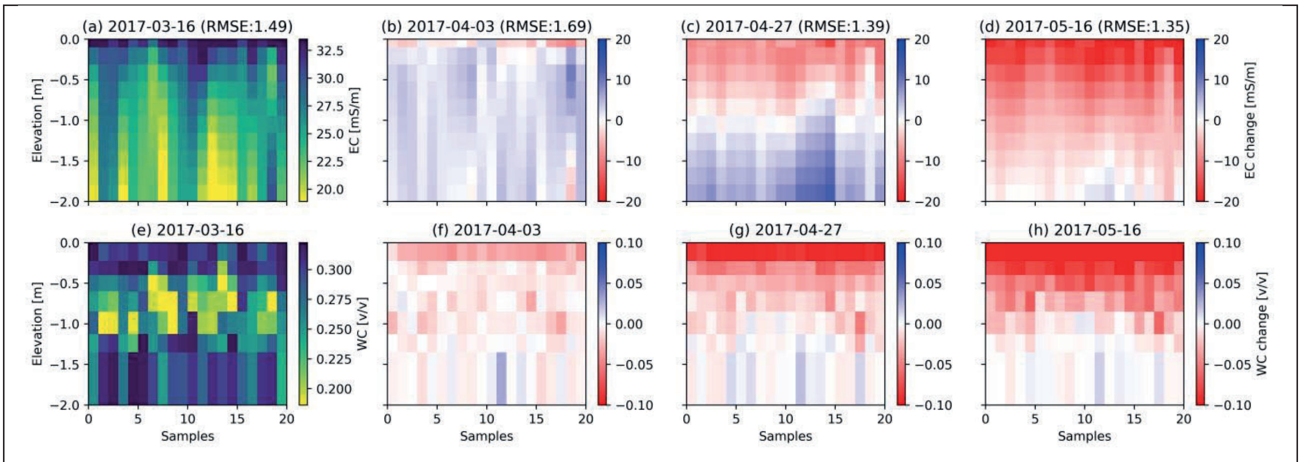

Figure 12: Evolution of the inverted change in electrical conductivity throughout the growth season (a to d) and of the measured soil moisture content (e to h). EC and WC changes are expressed as absolute difference relative to 2017-03-16 (models a and e). Deeper and larger decrease in EC is observed throughout the season mainly (b, c and d) following the change in soil moisture (f, g and h) mainly driven by root water uptake. Date format is YYYY-MM-DD (ISO 8601).

4 Conclusions

EMI has multiple applications to investigate the subsurface and is increasingly being used in multidisciplinary projects. EMagPy offers a user-friendly tool suitable for a broad range of applications. It was demonstrated that although the widely used CS forward model may perform well in low conductivity, homogeneous environments, the FS is often more appropriate. To help with the processing, modeling and inversion of EMI data, EMagPy has been developed. EMagPy is open-source software with an intuitive graphical user interface and Python API that enables flexible processing of EMI data. The use of EMagPy is demonstrated through several case studies exploring the limitations of the different forward models, ERT calibration, interface detection, effect of noise with height above ground and time-lapse inversion. The open-source nature and great flexibility of EMagPy makes it well suited for reproducible research and ideal for educational and training purposes.

Acknowledgments

We acknowledge the Hydrogeophysical Knowledge Exchange group, a partnership between Lancaster University (UK) and Rutgers University (US) for their friendly audience and insightful feedback on EMI methods. PM is supported by the NERC Envision Doctoral Training Program (GA/15S/004 S301) and GB by a studentship by the Graduate School for Environment (a collaboration between Lancaster University, Center for Ecology and Hydrology (CEH) and Rothamsted Research).

References

Abdu, H., D. A. Robinson, and S. B. Jones. 2007. “Comparing Bulk Soil Electrical Conductivity Determination Using the DUALEM-1S and EM38-DD Electromagnetic Induction Instruments.” *Soil Science Society of America Journal* 71 (1): 189–96. https://doi.org/10.2136/sssaj2005.0394.

Anderson, Walter L. 1979. “Numerical Integration of Related Hankel Transforms of Orders 0 and 1 by Adaptive Digital Filtering.” *Geophysics* 44 (7): 1287–1305.

Andrade, F. C. M., T. Fischer, and J. Valenta. 2016. “Study of Errors in Conductivity Meters Using the Low Induction Number Approximation and How to Overcome Them.” In *Near Surface Geoscience 2016-22nd European Meeting of Environmental and Engineering Geophysics*. Barcelona, Spain: EAGE. https://doi.org/10.3997/2214-4609.201602080.

Auken, Esben, Anders Vest Christiansen, Casper Kirkegaard, Gianluca Fiandaca, Cyril Schamper, Ahmad Ali Behroozmand, Andrew Binley, et al. 2015. “An Overview of a Highly Versatile Forward and Stable Inverse Algorithm for Airborne, Ground-Based and Borehole Electromagnetic and Electric Data.” *Exploration Geophysics* 46 (3): 223–35. https://doi.org/10.1071/EG13097.

Bardossy, A, and S K Singh. 2008. “Robust Estimation of Hydrological Model Parameters.” *Hydrol. Earth Syst. Sci.*, 11.

Beamish, David. 2011. “Low Induction Number, Ground Conductivity Meters: A Correction Procedure in the Absence of Magnetic Effects.” *Journal of Applied Geophysics* 75 (2): 244–53. https://doi.org/10.1016/j.jappgeo.2011.07.005.

Binley, Andrew, Sami Ullah, A. Louise Heathwaite, Catherine Heppell, Patrick Byrne, Katrina Lansdown, Mark Trimmer, and Hao Zhang. 2013. “Revealing the Spatial Variability of Water Fluxes at the Groundwater-Surface Water Interface: Spatial Variability of Groundwater-Surface Water Fluxes.” *Water Resources Research* 49 (7): 3978–92. https://doi.org/10.1002/wrcr.20214.

Blanchy, Guillaume, Sina Saneiyan, Jimmy Boyd, Paul McLachlan, and Andrew Binley. 2020. “ResIPy, an Intuitive Open Source Software for Complex Geoelectrical Inversion/Modeling.” *Computers & Geosciences* 137 (April): 104423. https://doi.org/10.1016/j.cageo.2020.104423.

Brosten, Troy R., Frederick D. Day-Lewis, Gregory M. Schultz, Gary P. Curtis, and John W. Lane. 2011. “Inversion of Multi-Frequency Electromagnetic Induction Data for 3D Characterization of Hydraulic Conductivity.” *Journal of Applied Geophysics* 73 (4): 323–35. https://doi.org/10.1016/j.jappgeo.2011.02.004.

Byrd, Richard H., Peihuang Lu, Jorge Nocedal, and Ciyou Zhu. 1995. “A Limited Memory Algorithm for Bound Constrained Optimization.” *SIAM Journal on Scientific Computing* 16 (5): 1190–1208.

Christiansen, Anders, Jesper Pedersen, Esben Auken, Niels Søe, Mads Holst, and Søren Kristiansen. 2016. “Improved Geoarchaeological Mapping with Electromagnetic Induction Instruments from Dedicated Processing and Inversion.” *Remote Sensing* 8 (12): 1022. https://doi.org/10.3390/rs8121022.

Corwin, D. L., and J. D. Rhoades. 1984. “Measurement of Inverted Electrical Conductivity Profiles Using Electromagnetic Induction.” *Soil Science Society of America Journal* 48 (2): 288–291.

Corwin, Dennis L. 2008. “Past, Present, and Future Trends in Soil Electrical Conductivity Measurements Using Geophysical Methods.” *Handbook of Agricultural Geophysics*, 17–44.

Dafflon, Baptiste, Susan S. Hubbard, Craig Ulrich, and John E. Peterson. 2013. “Electrical Conductivity Imaging of Active Layer and Permafrost in an Arctic Ecosystem, through Advanced Inversion of Electromagnetic Induction Data.” *Vadose Zone Journal* 12 (4).

Davies, Gareth, Jingyi Huang, Fernando Acacio Monteiro Santos, and John Triantafilis. 2015. “Modeling Coastal Salinity in Quasi 2D and 3D Using a DUALEM-421 and Inversion Software.” *Groundwater* 53 (3): 424–431.

Duan, Qingyun, Soroosh Sorooshian, and Vijai K. Gupta. 1994. “Optimal Use of the SCE-UA Global Optimization Method for Calibrating Watershed Models.” *Journal of Hydrology* 158 (3–4): 265–284.

Elwaseif, M., J. Robinson, F.D. Day-Lewis, D. Ntarlagiannis, L.D. Slater, J.W. Lane, B.J. Minsley, and G. Schultz. 2017. “A Matlab-Based Frequency-Domain Electromagnetic Inversion Code (FEMIC) with Graphical User Interface.” *Computers & Geosciences* 99 (February): 61–71. https://doi.org/10.1016/j.cageo.2016.08.016.

Farquharson, Colin G., Douglas W. Oldenburg, and Partha S. Routh. 2003. “Simultaneous 1D Inversion of Loop–Loop Electromagnetic Data for Magnetic Susceptibility and Electrical Conductivity” 68 (6): 1857–1869. https://doi.org/10.1190/1.1635038.

Frederiksen, Rasmus Rumph, Anders Vest Christiansen, Steen Christensen, and Keld Rømer Rasmussen. 2017. “A Direct Comparison of EMI Data and Borehole Data on a 1000ha Data Set.” *Geoderma* 303 (October): 188–95. https://doi.org/10.1016/j.geoderma.2017.04.028.

Frischknecht, F. C. 1987. “Electromagnetic Physical Scale Modeling.” *Electromagnetic Methods in Applied Geophysics-Theory*, 365–441.

Gebbers, Robin, Erika Lück, Michel Dabas, and Horst Domsch. 2009. “Comparison of Instruments for Geoelectrical Soil Mapping at the Field Scale.” *Near Surface Geophysics* 7 (3): 179–90. https://doi.org/10.3997/1873-0604.2009011.

Guillemoteau, Julien, Pascal Sailhac, Charles Boulanger, and Jérémie Trules. 2015. “Inversion of Ground Constant Offset Loop-Loop Electromagnetic Data for a Large Range of Induction Numbers.” *GEOPHYSICS* 80 (1): E11–21. https://doi.org/10.1190/geo2014-0005.1.

Guptasarma, D., and B. Singh. 1997. “New Digital Linear Filters for Hankel J0 and J1 Transforms.” *Geophysical Prospecting* 45 (5): 745–762.
Hanssens, Daan, Samuël Delefortrie, Christin Bobe, Thomas Hermans, and Philippe De Smedt. 2019. “Improving the Reliability of Soil EC-Mapping: Robust Apparent Electrical Conductivity (RECa) Estimation in Ground-Based Frequency Domain Electromagnetics.” *Geoderma* 337 (March): 1155–63. https://doi.org/10.1016/j.geoderma.2018.11.030.
Heagy, Lindsey J., Rowan Cockett, Seogi Kang, Gudni K. Rosenkjaer, and Douglas W. Oldenburg. 2017. “A Framework for Simulation and Inversion in Electromagnetics.” *Computers & Geosciences* 107 (October): 1–19. https://doi.org/10.1016/j.cageo.2017.06.018.
Hebel, Christian von, Sebastian Rudolph, Achim Mester, Johan A. Huisman, Pramod Kumbhar, Harry Vereecken, and Jan van der Kruk. 2014. “Three-Dimensional Imaging of Subsurface Structural Patterns Using Quantitative Large-Scale Multiconfiguration Electromagnetic Induction Data.” *Water Resources Research* 50 (3): 2732–48. https://doi.org/10.1002/2013WR014864.
Houska, Tobias, Philipp Kraft, Alejandro Chamorro-Chavez, and Lutz Breuer. 2015. “SPOTting Model Parameters Using a Ready-Made Python Package.” *PloS One* 10 (12): e0145180.
Huang, H, and I Won. 2000. “Conductivity and Susceptibility Mapping Using Broadband Electromagnetic Sensors.” *Journal of Environmental and Engineering Geophysics*, 12.
Huang, J., F.A. Monteiro Santos, and J. Triantafilis. 2016. “Mapping Soil Water Dynamics and a Moving Wetting Front by Spatiotemporal Inversion of Electromagnetic Induction Data,” November. https://doi.org/10.1002/2016WR019330.
Huang, J., A. Pedrera-Parrilla, K. Vanderlinden, E.V. Taguas, J.A. Gómez, and J. Triantafilis. 2017. “Potential to Map Depth-Specific Soil Organic Matter Content across an Olive Grove Using Quasi-2d and Quasi-3d Inversion of DUALEM-21 Data.” *CATENA* 152 (May): 207–17. https://doi.org/10.1016/j.catena.2017.01.017.
Huang, Jingyi, Alfred E. Hartemink, Francisco Arriaga, and Nathaniel W. Chaney. 2019. “Unraveling Location-Specific and Time-Dependent Interactions between Soil Water Content and Environmental Factors in Cropped Sandy Soils Using Sentinel-1 and Moisture Probes.” *Journal of Hydrology* 575 (August): 780–93. https://doi.org/10.1016/j.jhydrol.2019.05.075.
Jadoon, Khan Zaib, Davood Moghadas, Aurangzeb Jadoon, Thomas M. Missimer, Samir K. Al-Mashharawi, and Matthew F. McCabe. 2015. “Estimation of Soil Salinity in a Drip Irrigation System by Using Joint Inversion of Multicoil Electromagnetic Induction Measurements.” *Water Resources Research* 51 (5): 3490–3504. https://doi.org/10.1002/2014WR016245.
Koganti, Triven, Bhaskar Narjary, Ehsan Zare, Aslam Latif Pathan, Jingyi Huang, and John Triantafilis. 2018. “Quantitative Mapping of Soil Salinity Using the DUALEM-21S Instrument and EM Inversion Software.” *Land Degradation & Development* 29 (6): 1768–81. https://doi.org/10.1002/ldr.2973.
Laloy, E., M. Weynants, C.L. Bielders, M. Vanclooster, and M. Javaux. 2010. “How Efficient Are One-Dimensional Models to Reproduce the Hydrodynamic Behavior of Structured Soils Subjected to Multi-Step Outflow Experiments?” *Journal of Hydrology* 393 (1–2): 37–52. https://doi.org/10.1016/j.jhydrol.2010.02.017.

Lavoué, F., J. Van Der Kruk, J. Rings, F. André, D. Moghadas, J. A. Huisman, S. Lambot, L. Weihermüller, Jan Vanderborght, and H. Vereecken. 2010. “Electromagnetic Induction Calibration Using Apparent Electrical Conductivity Modelling Based on Electrical Resistivity Tomography.” *Near Surface Geophysics* 8 (6): 553–561.

Martinelli, Patricia, and María Celeste Duplaá. 2008. “Laterally Filtered 1D Inversions of Small-Loop, Frequency-Domain EMI Data from a Chemical Waste Site.” *Geophysics* 73 (4): F143–F149.

Martini, Edoardo, Ulrike Werban, Steffen Zacharias, Marco Pohle, Peter Dietrich, and Ute Wollschläger. 2017. “Repeated Electromagnetic Induction Measurements for Mapping Soil Moisture at the Field Scale: Validation with Data from a Wireless Soil Moisture Monitoring Network.” *Hydrology and Earth System Sciences* 21 (1): 495–513. https://doi.org/10.5194/hess-21-495-2017.

McNeill, J. D. 1980. *Electromagnetic Terrain Conductivity Measurement at Low Induction Numbers*. Geonics Limited Ontario, Canada. http://www.geonics.com/pdfs/technicalnotes/tn6.pdf.

Moghadas, Davood, Frédéric André, John H. Bradford, Jan van der Kruk, Harry Vereecken, and Sébastien Lambot. 2012. “Electromagnetic Induction Antenna Modelling Using a Linear System of Complex Antenna Transfer Functions.” *Near Surface Geophysics* 10 (3): 237–47. https://doi.org/10.3997/1873-0604.2012002.

Monteiro Santos, Fernando A. 2004. “1-D Laterally Constrained Inversion of EM34 Profiling Data.” *Journal of Applied Geophysics* 56 (2): 123–34. https://doi.org/10.1016/j.jappgeo.2004.04.005.

Nelder, John A., and Roger Mead. 1965. “A Simplex Method for Function Minimization.” *The Computer Journal* 7 (4): 308–313.

Nüsch, Anne-Kathrin, Peter Dietrich, Ulrike Werban, and Thorsten Behrens. 2010. “Acquisition and Reliability of Geophysical Data in Soil Science,” 4.

Pedersen, J. B., E. Auken, A. V. Christiansen, and S. M. Kristiansen. 2015. “Mapping Soil Heterogeneity Using Spatially Constrained Inversion of Electromagnetic Induction Data.” In *First Conference on Proximal Sensing Supporting Precision Agriculture*, 2015:1–5. European Association of Geoscientists & Engineers.

Robinson, David A., Hiruy Abdu, Inma Lebron, and Scott B. Jones. 2012. “Imaging of Hill-Slope Soil Moisture Wetting Patterns in a Semi-Arid Oak Savanna Catchment Using Time-Lapse Electromagnetic Induction.” *Journal of Hydrology* 416–417 (January): 39–49. https://doi.org/10.1016/j.jhydrol.2011.11.034.

Rücker, Carsten, Thomas Günther, and Florian M. Wagner. 2017. “PyGIMLi: An Open-Source Library for Modelling and Inversion in Geophysics.” *Computers & Geosciences* 109 (December): 106–23. https://doi.org/10.1016/j.cageo.2017.07.011.

Saey, Timothy, Jeroen Verhegge, Philippe De Smedt, Marthe Smetryns, Nicolas Note, Ellen Van De Vijver, Pieter Laloo, Marc Van Meirvenne, and Samuël Delefortrie. 2016. “Integrating Cone Penetration Testing into the 1D Inversion of Multi-Receiver EMI Data to Reconstruct a Complex Stratigraphic Landscape.” *CATENA* 147 (December): 356–71. https://doi.org/10.1016/j.catena.2016.07.023.

Shanahan, Peter W., Andrew Binley, W. Richard Whalley, and Christopher W. Watts. 2015. “The Use of Electromagnetic Induction to Monitor Changes in Soil Moisture Profiles beneath Different Wheat Genotypes.” *Soil Science Society of America Journal* 79 (2): 459. https://doi.org/10.2136/sssaj2014.09.0360.

Sherlock, Mark D., and Jeffrey J. McDonnell. 2003. “A New Tool for Hillslope Hydrologists: Spatially Distributed Groundwater Level and Soilwater Content Measured Using Electromagnetic Induction.” *Hydrological Processes* 17 (10): 1965–1977.
Sudduth, K. A., S. T. Drummond, and N. R. Kitchen. 2001. “Accuracy Issues in Electromagnetic Induction Sensing of Soil Electrical Conductivity for Precision Agriculture.” *Computers and Electronics in Agriculture* 31 (3): 239–264.
Tan, Xhie. 2019. “SIMULTANEOUS CALIBRATION AND INVERSION ALGORITHM FOR MULTI-CONFIGURATION ELECTROMAGNETIC INDUCTION DATA ACQUIRED AT MULTIPLE ELEVATIONS,” 55.
Triantafilis, J., G. M. Laslett, and A. B. McBratney. 2000. “Calibrating an Electromagnetic Induction Instrument to Measure Salinity in Soil under Irrigated Cotton.” *Soil Science Society of America Journal* 64 (3): 1009–1017.
Triantafilis, John, and S. M. Lesch. 2005. “Mapping Clay Content Variation Using Electromagnetic Induction Techniques.” *Computers and Electronics in Agriculture* 46 (1–3): 203–237.
Van Der Kruk, J., J. A. C. Meekes, P. M. Van Den Berg, and J. T. Fokkema. 2000. “An Apparent-Resistivity Concept for Low-Frequency Electromagnetic Sounding Techniques.” *Geophysical Prospecting* 48 (6): 1033–1052.
Virtanen, Pauli, Ralf Gommers, Travis E. Oliphant, Matt Haberland, Tyler Reddy, David Cournapeau, Evgeni Burovski, et al. 2020. “SciPy 1.0: Fundamental Algorithms for Scientific Computing in Python.” *Nature Methods* 17 (3): 261–72. https://doi.org/10.1038/s41592-019-0686-2.
von Hebel, van der Kruk, Huisman, Mester, Altdorff, Endres, Zimmermann, Garré, and Vereecken. 2019. “Calibration, Conversion, and Quantitative Multi-Layer Inversion of Multi-Coil Rigid-Boom Electromagnetic Induction Data.” *Sensors* 19 (21): 4753. https://doi.org/10.3390/s19214753.
Vrugt, J. A., and C. J. F. Ter Braak. 2011. “DREAM(D): An Adaptive Markov Chain Monte Carlo Simulation Algorithm to Solve Discrete, Noncontinuous, and Combinatorial Posterior Parameter Estimation Problems.” *Hydrology and Earth System Sciences* 15 (12): 3701–3713. https://doi.org/10.5194/hess-15-3701-2011.
Wait, James R. 1982. *Geo-Electromagnetism*. Academic Press. New York.
Whalley, W.R., A. Binley, C.W. Watts, P. Shanahan, I.C. Dodd, E.S. Ober, R.W. Ashton, C.P. Webster, R.P. White, and M. J. Hawkesford. 2017. “Methods to Estimate Changes in Soil Water for Phenotyping Root Activity in the Field.” *Plant and Soil* 415 (1–2): 407–22. https://doi.org/10.1007/s11104-016-3161-1.
Williams, B. G., and G. C. Baker. 1982. “An Electromagnetic Induction Technique for Reconnaissance Surveys of Soil Salinity Hazards.” *Soil Research* 20 (2): 107–18. https://doi.org/10.1071/sr9820107.
Zare, E., A. Beucher, J. Huang, A. Boman, S. Mattbäck, M. H. Greve, and J. Triantafilis. 2018. “Three-Dimensional Imaging of Active Acid Sulfate Soil Using a DUALEM-21S and EM Inversion Software.” *Journal of Environmental Management* 212: 99–107.
Zare, E., J. Huang, F. A. Santos, and J. Triantafilis. 2015. “Mapping Salinity in Three Dimensions Using a DUALEM-421 and Electromagnetic Inversion Software.” *Soil Science Society of America Journal* 79 (6): 1729–1740.

Appendix A

Table A1. Main API methods used in EMagPy.

`Problem.show()`	Show apparent values as scatter plot
`Problem.showMap()`	Show spatial distribution of apparent values for given coil
`Problem.calibrate()`	Calibration of ECa value given depth-specific EC dataset
`Problem.invert()`	General inversion routine
`Problem.showResults()`	Show inversion results as a transect
`Problem.showSlice()`	Show the slice for the selected inverted layer
`Problem.showOne2one()`	Show 1:1 graph of modeled vs observed apparent EC
`Problem.showMisfit()`	Show the observed and the modeled ECa